Plastic Strains and Energy Density in Cracked Plates

Part I*—Experimental Technique and Results

To facilitate presentation of data and comparison to available theory, this paper is divided into two parts: the first is primarily concerned with experimental procedure and results; and the second is concerned with correlation of data to elastic theory and a discussion of ductile fracture in light of experimental evidence

by William W. Gerberich

ABSTRACT—A technique is presented which allows separation of the principal plastic strains within an enclave at a crack tip in relatively thin plates. For plates with a number of crack lengths, several degrees of tensile loading are applied to five ductile materials with widely varying mechanical properties. Principal plastic strain distributions, plastic distortional strain energy density and total plastic energy are determined within the resulting plastic enclaves. It is shown that the degree of loading and strain hardening greatly affect the principal plastic strain and energy density distributions and that this is reflected in the amount of strain energy that can be plastically absorbed at a crack tip.

Nomenclature

a = half crack length
ΔA = incremental area within enclave
$\epsilon_1, \epsilon_2, \epsilon_3$ = principal plastic strains
δ = relative retardation of 2.27×10^{-5} in. corresponding to first fringe order
E = tensile modulus of elasticity
F = loading factor defined in eq (7)
γ_{oct} = octahedral shear strain
k = strain optical coefficient
n = strain-hardening exponent
r, θ = polar coordinates
r_{max} = distance from crack tip along maximum extension of enclave
r_p = arbitrary value to define elastic-plastic boundary
$r_p(\theta)$ = shape of enclave
r_p' = maximum extension of enclave measured at $\epsilon_1 = 2000$ μin./in.
$r_\theta = 0°$ = distance from crack tip along line of crack extension
σ_0 = applied stress, gross section
σ_{ys} = uniaxial yield stress
t = plate thickness
t_c = thickness of photoelastic coating
τ_{oct} = octahedral shear stress
U_p = plastic strain energy in one enclave
w = plate width
W_d = plastic distortional strain energy density

William W. Gerberich is Senior Research Scientist, Philco Research Laboratory, Ford Motor Co., Newport Beach, Calif.

Paper was presented at the 1964 SESA Spring Meeting held in Salt Lake City, Utah on May 6–8.

**Part II of this paper will be published in the December 1964 issue of* EXPERIMENTAL MECHANICS.

Introduction

Before 1950, a large amount of information was obtained pertaining to completely elastic and completely plastic problems. Considerably less information was available concerning combined elastic-plastic deformation; in particular, a full description of both the stresses and strains in the neighborhood of a crack tip was lacking. Such information, however, would be of great value, as suggested by a partial list of the recent publications[1–17] devoted to this problem.

The analytical and numerical solutions of Hult and McClintock[1, 2] and Koskinen[3] consider plasticity at the tips of shear cracks. Several numerical solutions are available for the plane problems. Allen and Southwell[4] have examined the plastic enclave for stresses and displacements at the tip of an edge vee-notch in the case of both plane stress and plane strain. Stimpson and Eaton[5] have determined the plastic enclave for a straight-edge cut in a flat plate but only considered the stresses. A similar analysis was made for the plane-strain case by Jacobs.[6] Experimentally, there have been a number of investigations of plastic enclaves such as the photoelastic studies of Kawata,[7] Dixon,[8] and Ault.[9] These studies, however, did not separate the principal strains throughout the enclave. Two experi-

mental studies, one by Liu and Carpenter[10] and one by Weiss, *et al.*,[11] separated the principal strains but, in the first case, very large deformations were observed in a $^3/_4$-in.-thick plate which involved considerable triaxiality, and, in the second, the investigation was limited to relatively large deformations along the line of the crack.

Thus, there have been no analytical solutions and relatively few numerical or experimental results on the strains within a plastic enclave at the tip of a crack under normal stress. As a result, for fracture criteria, about the only available information has been the planar elastic solutions typified by the work of Inglis,[12] Westergaard,[13] and Williams[14] and a family of energy criteria derived from those typified by Griffith,[15] Orowan,[16] and Irwin.[17] For fracture of very ductile materials, further information is necessary as a first step to extend these criteria or to generate new ones.

Therefore, an experimental technique was devised to separate the principal plastic strains within the enclave and thereby determine the plastic energy density distribution and total plastic strain energy in it. An extensive experimental program studying these parameters as a function of applied stress and crack length was conducted. Also, since none of the numerical solutions considered strain hardening and since no quantitative deductions could be drawn from existing experimental data on the effects of strain hardening, a number of materials with widely varying strain-hardening properties were studied.

To facilitate presentation of the data and comparison to available theory, this document has been divided into two parts: the first being primarily concerned with the experimental procedure and results, and the second being concerned with correlation of data to elastic theory and a discussion of ductile fracture in light of the experimental evidence.

Experimental Procedure

Since strain hardening and other material properties were to be studied, the following materials with widely varying properties were chosen: 2024-0 aluminum, 6061-T6 aluminum, AZ-31B-H24 magnesium, 4340 normalized steel and 7075-T6 aluminum. From sheet specimens of each material, engineering stress–strain curves, true stress–true strain curves and strain-hardening coefficients were determined.

To obtain plastic deformation at the tips of cracks, a 3-in.-wide test coupon with an internal crack was loaded to a predetermined stress level, and then unload. In analyzing the plastic strains of the resulting enclave, a photoelastic-coating method used by Kawata[7] was utilized in conjunction with the measurement of thickness strains. Test coupons 3-in. wide by 12-in. long were made with crack sizes ranging from 0.2 to 1.5 in.; at each end of a relatively large slot, simulated cracks with root radii less than or equal to 0.001 in. were produced by electrical-discharge machining. The nominal thickness of all test coupons was 0.10 in., so that the influence of thickness was ignored except where energy was determined. A photoelastic coating having identical boundary conditions was bonded to the surface of each specimen, following an established method.[18] After the specimen was loaded to the desired applied stress, it was unloaded, and the residual plastic deformation as indicated by the isochromatics in the birefringent coating was measured using a reflective polariscope. The zone thus observed is termed a plastic enclave, following Allen and Southwell.[4] Using several combinations of the polarizer and analyzer, the birefringence was recorded in at least half- and full-order fringes using both color and black and white photography. From the well-known strain-optical photoelastic law for coatings,

$$\epsilon_1 - \epsilon_2 = \delta/2kt_c \qquad (1)$$

the principal plastic strain difference contours were determined. On an average, the strain optical coefficient, k, was 0.060, and the thickness of the coating was 0.10 in., allowing estimates of $\epsilon_2 - \epsilon_2$ to be made within 200 μin./in. The accuracy of the measurement in regions of large strains was 10 percent or better. The principal strain differences were evaluated at 0.05- or 0.10-in. intervals on one quadrant of the plate, the spacing depending upon the plastic-enclave size.

After the isochromatics were recorded, the photoelastic coating was carefully stripped from the specimen and the thickness of the plate was determined at each mesh point, i.e., where the principal strain differences were found. Using a Zeiss Orthotest mechanical comparator, thickness differences of 2×10^{-5} in. could be estimated. Using the initial thickness of the plate, calculation of the average principal strain through the thickness, ϵ_3, followed directly.

In the regions of large plastic deformation, the accuracy was within 10 percent, being commensurate with the photoelastic measurements. Assuming the incompressibility condition, $\epsilon_1 + \epsilon_2 + \epsilon_3 = 0$, and using the measurements of $\epsilon_1 - \epsilon_2$ and ϵ_3, the individual principal strains in the plastic enclave can be readily resolved.

Once the principal strains were separated, the octahedral shear strain, the plastic strain energy density, W_d, and the total plastic energy, U_p, were determined. The octahedral shear strain is defined as

$$\gamma_{oct} = {}^2/_3 \sqrt{(\epsilon_1 - \epsilon_2)^2 + (\epsilon_2 - \epsilon_3)^2 + (\epsilon_3 - \epsilon_1)^2} \qquad (2)$$

from which γ_{oct} was computed at each mesh point. The distortional strain energy density is defined as

$$W_d = \int_0^{\gamma_{oct}} \tau_{oct} d\gamma_{oct} \qquad (3)$$

and may be determined from the stress–strain data appropriate to the material under consideration. This enabled determination of a generalized plane-stress value of the plastic distortional strain energy

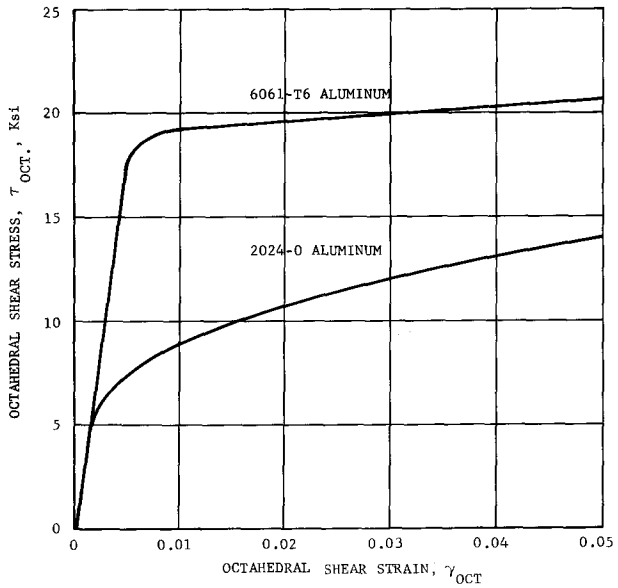

Fig. 1—Octahedral stress-strain curves for 6061-T6 and 2024-0 aluminum alloys

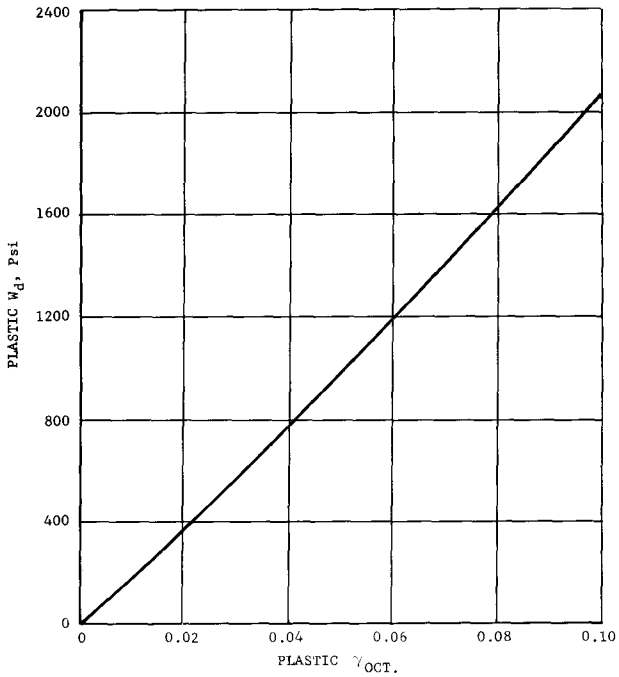

Fig. 2—Plastic distortional strain energy density as a function of plastic octahedral shear strain for 6061-T6 aluminum

density per unit thickness at each point of the quadrant. By definition, the total plastic energy of the entire enclave in half of the plate is next determined from

$$U_p = t \int_0^{2\pi} \int_0^{r_p(\theta)} W_d(r,\theta) r \, dr \, d\theta \cong t \sum_{\text{mesh}} w_d \, \Delta A \quad (4)$$

Actually, U_p was determined from the approximation by summing W_d for equal increments of ΔA over the entire enclave in half of the plate.

Verification of Test Procedure

For very small or no plastic deformations, the elastic stress distribution should be approximated during loading. The author[18] has used the photoelastic-coating method to examine the stress distribution about cracks in elastic plates. High-strength steel specimens which had yield strengths about 250 ksi were loaded within the elastic regime only. It was shown that the stress distribution determined from the photoelastic analysis was very close to that predicted by numerical[20] and electrical-analog[21] solutions. Both the shape of the isochromatics and their magnitude were almost identical to the numerical solutions, even very close to the crack tip.

Also, the procedure for photoelastically determining values of $\epsilon_1 - \epsilon_2$ in a specimen that underwent large plastic deformations was verified.[18] A photoelastic coating was applied to a sheet of 2024-0 aluminum, loaded so that yielding had occurred across the net section and then unloaded.

TABLE 1—TENSILE DATA FOR MATERIALS OF THIS INVESTIGATION

Material	0.2% offset yield stress, ksi	Tensile stress, ksi	Elongation in 2 in., %	Reduction of area, %	True stress at fracture, ksi	True strain at fracture, %	Strain-hardening exponent, n
2024-O Aluminum	15.4	34.7	17.5	28.4	45.3	33.3	0.250
	15.4	34.6	15.0	20.4*	40.6*	23.1*	
6061-T6 Aluminum	41.3	42.7	11.0	43.6	63.0	57.1	0.068
	39.6	43.5	10.5	39.2	59.2	49.5	
AZ-31B—H24 Magnesium	31.8	42.8	13.0	16.8	51.4	18.4	0.215†
	31.6	42.8	12.0	14.3	50.0	15.6	
4340-Normalized steel	62.0	91.2	24.0	45.3	129.0	60.5	0.145
	59.1	92.5	24.0	43.9	127.0	58.0	
7075-T6 Aluminum	70.1	81.4	11.0	20.4	99.0	22.7	0.080
	70.1	81.4	11.0	20.5	99.0	23.1	

* Fractured at gage mark.
† Averaged value—see Fig. 3.

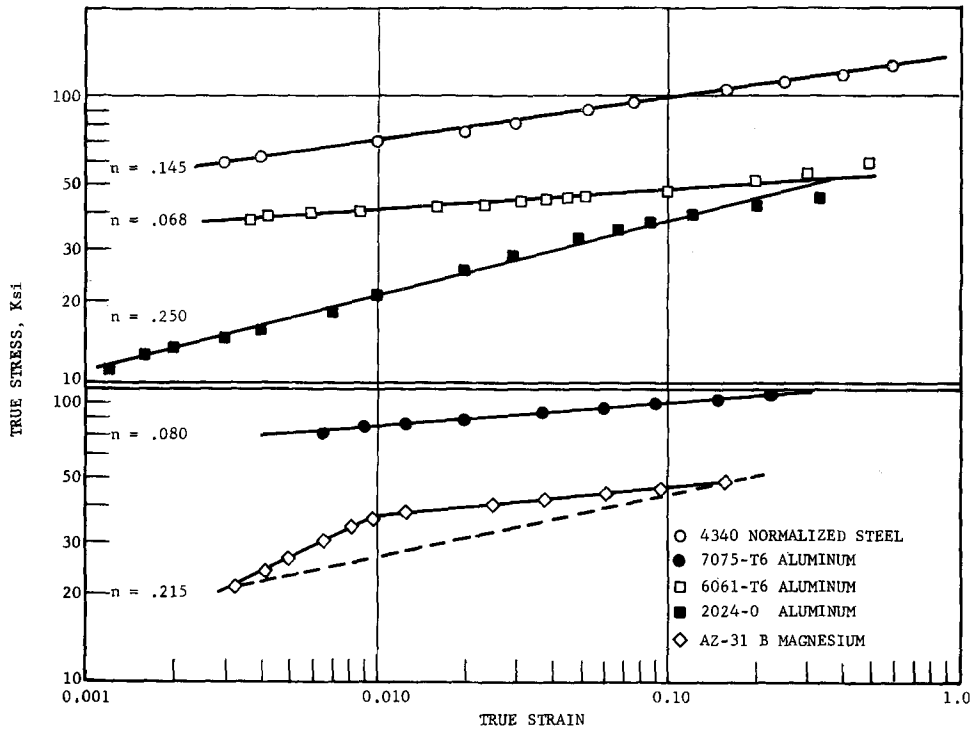

Fig. 3—True stress–true strain log-log plots for all materials

After isochromatic fringes were recorded, the bonded plastic was milled down to one-half its original thickness, again recording the fringes. After repeating this procedure once more, the fringe order was determined at several distances from the crack tip for each plastic thickness. Extrapolating to zero plastic thickness, the data clearly showed that errors in determining $\epsilon_1 - \epsilon_2$ with 0.1-in.-thick plastic were less than 10 percent, even as close to the crack tip as 0.05 in. Thus, it is seen that this photoelastic method is reasonable for determining the principal strain differences at distances from the crack tip greater than the thickness of the material for deformations ranging from the purely elastic to very large plastic ones.

It was necessary to know whether residual stresses affected the measurements in the resulting plastic enclaves. A specimen was loaded into the plastic regime and then unloaded (as described earlier), the isochromatics being recorded. The specimen was carefully cut along the boundary of the enclave to relieve any residual stresses in that area. No change in the isochromatics was noted, indicating that residual-stress effects were of secondary importance.

Experimental Results

Tensile results for investigated materials are shown in Table 1. It is seen that the materials chosen have a wide range of properties as indicated by the variation in strength, strain hardening and ductility. The true stress–true strain characteristic of each material was used to determine each of the $\tau_{oct} - \gamma_{oct}$ curves. The octahedral curves are shown in Fig. 1 for the two materials which exhibited the extremes in strain-hardening behavior. To facilitate determination of energy density in the cracked plates, plastic strain energy density was found as a function of plastic octahedral-shear strain from tensile data. This is shown in Fig. 2 for the 6061-T6 aluminum and is seen to be a relatively linear relation for this low strain-hardening material. Also determined from the true stress–true strain curves were the strain-hardening exponents for each material. As seen in Fig. 3, the log-log plots resulted in relatively straight lines for all materials except the magnesium alloy, which seemed to have two distinct regions of strain hardening. To simplify the correlation of results, it was assumed that this material had an average strain-hardening exponent determined by the slope drawn through the beginning and end points of plastic deformation.

Plastic enclaves of various sizes and shapes were obtained by loading twenty center-cracked tensile specimens of the five materials. The various loading and geometrical parameters for each specimen are given in Table 2. The stress–strain characteristics of a material had an effect on the resulting plastic enclave, as may be seen qualitatively in Fig. 4. Here, isochromatics for three plastic enclaves of about the same size are shown. On the left is 2024-0 aluminum which has a strain-hardening exponent $n = 0.250$; in the middle is 6061-T6 aluminum ($n = 0.068$); and on the right is mild steel which demonstrates a yield-point instability. The latter is shown through the courtesy of J. R. Dixon.[8] It is

TABLE 2—EXPERIMENTAL DATA FOR PLASTIC ENCLAVES

Material	Thick, in.	Yield stress, σ_{ys}, ksi	Applied stress, σ_0, ksi	Crack length, 2a, in.	F*	Plastic† enclave size, r_p', in.	Plastic‡ energy, U_p, in.-lb
061-T6 Aluminum	0.0994	40.4	36.1	0.200	0.168	0.115	0.535
	0.0996	40.4	26.6	0.780	0.366	0.169	0.920
	0.0993	40.4	18.6	1.52	0.384	0.211	1.09
	0.0995	40.4	27.8	0.780	0.398	0.223	1.76
	0.0980	40.4	29.6	0.700	0.410	0.247	1.82
	0.0992	40.4	19.8	1.53	0.442	0.293	2.17
	0.0995	40.4	21.2	1.53	0.505	1.05	8.47
7075-T6 Aluminum	0.1002	70.1	45.4	0.220	0.096	0.026	0.290
	0.1010	70.1	30.3	0.780	0.157	0.088	0.340
	0.1008	70.1	21.2	1.53	0.164	0.116	0.560
	0.1001	70.1	41.0	0.775	0.285	0.134	1.13
4340 Normalized steel	0.1260	60.6	42.7	0.785	0.422	0.204	2.10
	0.1282	60.6	30.8	1.52	0.476	0.256	2.42
	0.1282	60.6	34.0	1.52	0.582	0.616	10.2
	0.1281	60.6	52.5	0.800	0.654	1.02	22.4
	0.1284	60.6	38.6	1.53	0.748	~2.0§	76.0
AZ-31B Magnesium	0.1010	31.7	19.7	1.00	0.425	0.142	0.500
	0.1001	31.7	21.4	1.05	0.530	0.275	2.34
2024-O Aluminum	0.0937	15.4	11.1	0.965	0.546	0.144	0.365
	0.0930	15.4	13.7	1.00	0.870	0.654	2.34

* $F = (\sigma_0/\sigma_{ys})^2 \left[\frac{\pi a}{W} + \tan\left(\frac{\pi a}{W}\right)\right]$.
† Measured at maximum extension of ($\epsilon_1 = 2000$ μin./in.
‡ Plastic energy absorbed in one whole enclave or half the plate.
§ Extrapolated.

evident that as the strain hardening decreases, the enclave tends to become more pointed. Quantitative measurements of the principal strain distributions, ϵ_1, ϵ_2 and ϵ_3, are shown for three materials with varying degrees of strain hardening in Fig. 5. In all cases, the shape and magnitude of the ϵ_1 contours are very similar to those of the ϵ_3 contours for each material. As will be shown in Part II,[19] the shape of principal strain contours for the high strain-hardening material, 2024-0 aluminum, are closely approximated by the exact elastic solution of Inglis. Thus, as the strain hardening decreases, there is a strong tendency to deviate from the elastic solution for the enclaves to become more pointed and to become oriented closer to the line of the crack.

How the enclave shape varies with strain hardening is more clearly seen in Fig. 6, where the ratio of the maximum extension of the enclave, r_{max}, to the extension of the enclave along the line of the crack, $r_\theta = 0°$, is plotted vs. the magnitude of the larger in-plane principal strain, ϵ_1. As the strain hardening decreases, the enclave ratio becomes larger near the elastic-plastic interface, indicating a much more pointed enclave. However, very near the crack tip there is a smaller effect of strain hardening on the shape of the enclave. In Fig. 7, the effect of strain

Fig. 4—Isochromatic of plastic enclaves for 2024-0 aluminum, 6061-T6 aluminum and mild steel

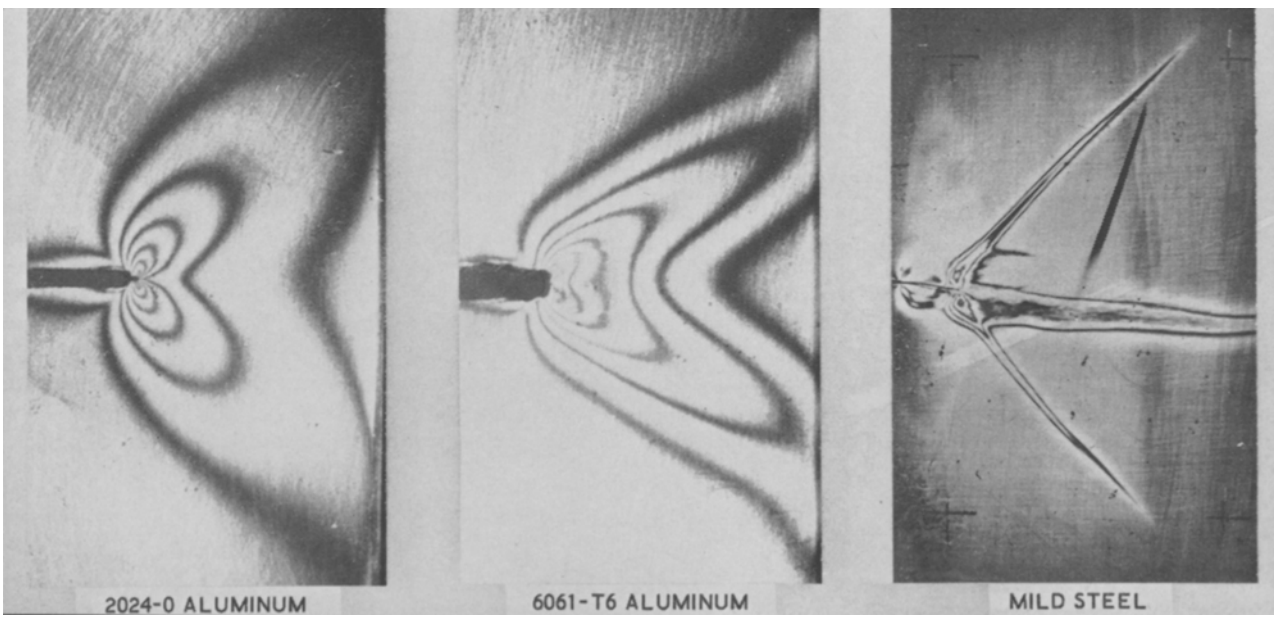

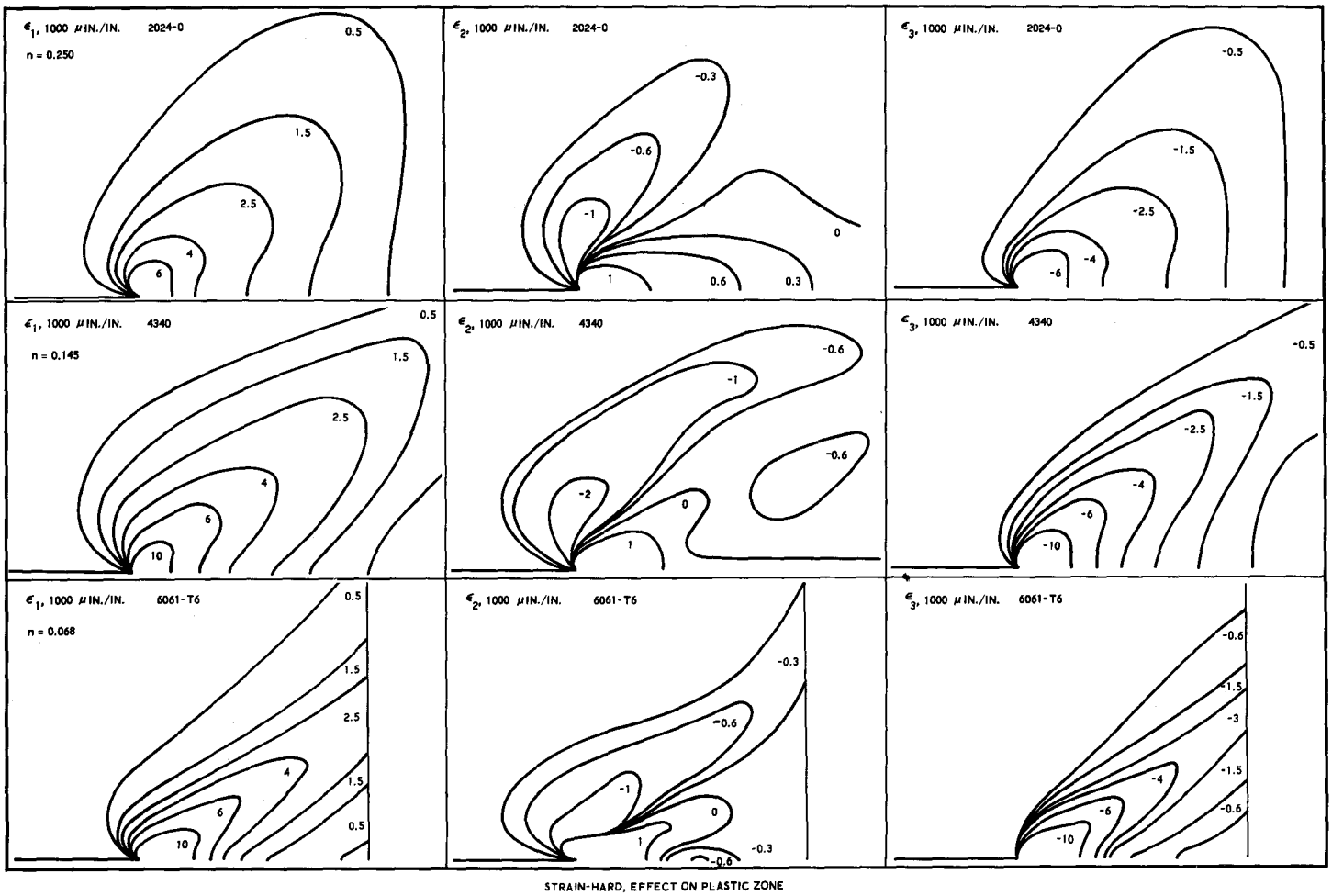

Fig. 5—Principal plastic strain distributions for 2024-0 aluminum, 4340 normalized steel and 6061-T6 aluminum

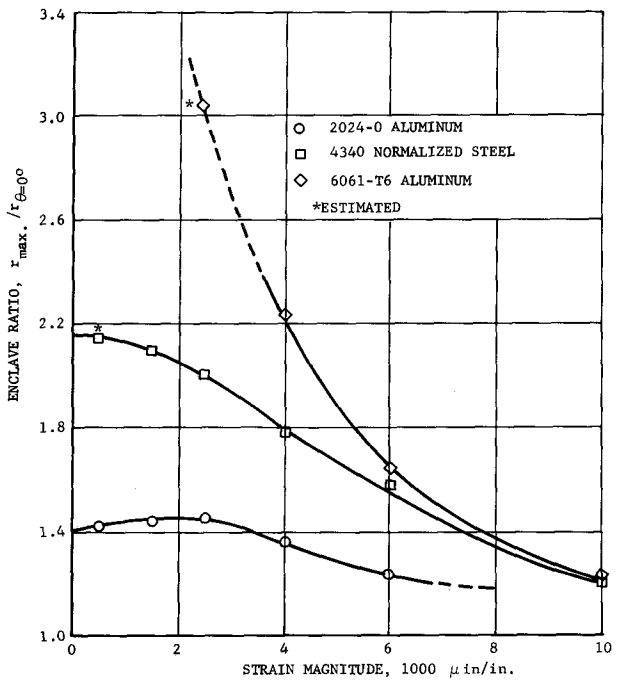

Fig. 6—Variation of enclave shape with strain hardening

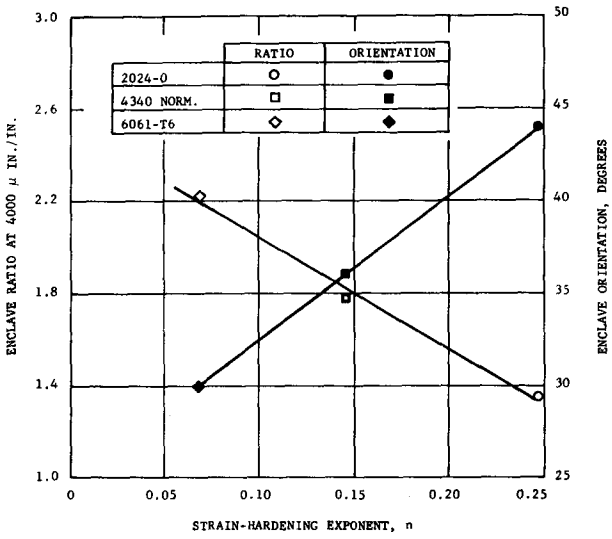

Fig. 7—Effect of strain hardening on enclave shape and orientation

hardening on both shape and orientation indicates that the enclave ratio decreases linearly and the enclave orientation increases linearly with increasing strain hardening. For a different strain magnitude and for larger or smaller degrees of strain hardening, the behavior for shape and orientation would probably deviate from this linear behavior. Also, similar effects may not be observed for specimens with different thicknesses.

Besides strain hardening, there is also a strong effect of load level as is evidenced by the relative enclave size on the shape of the strain contours.

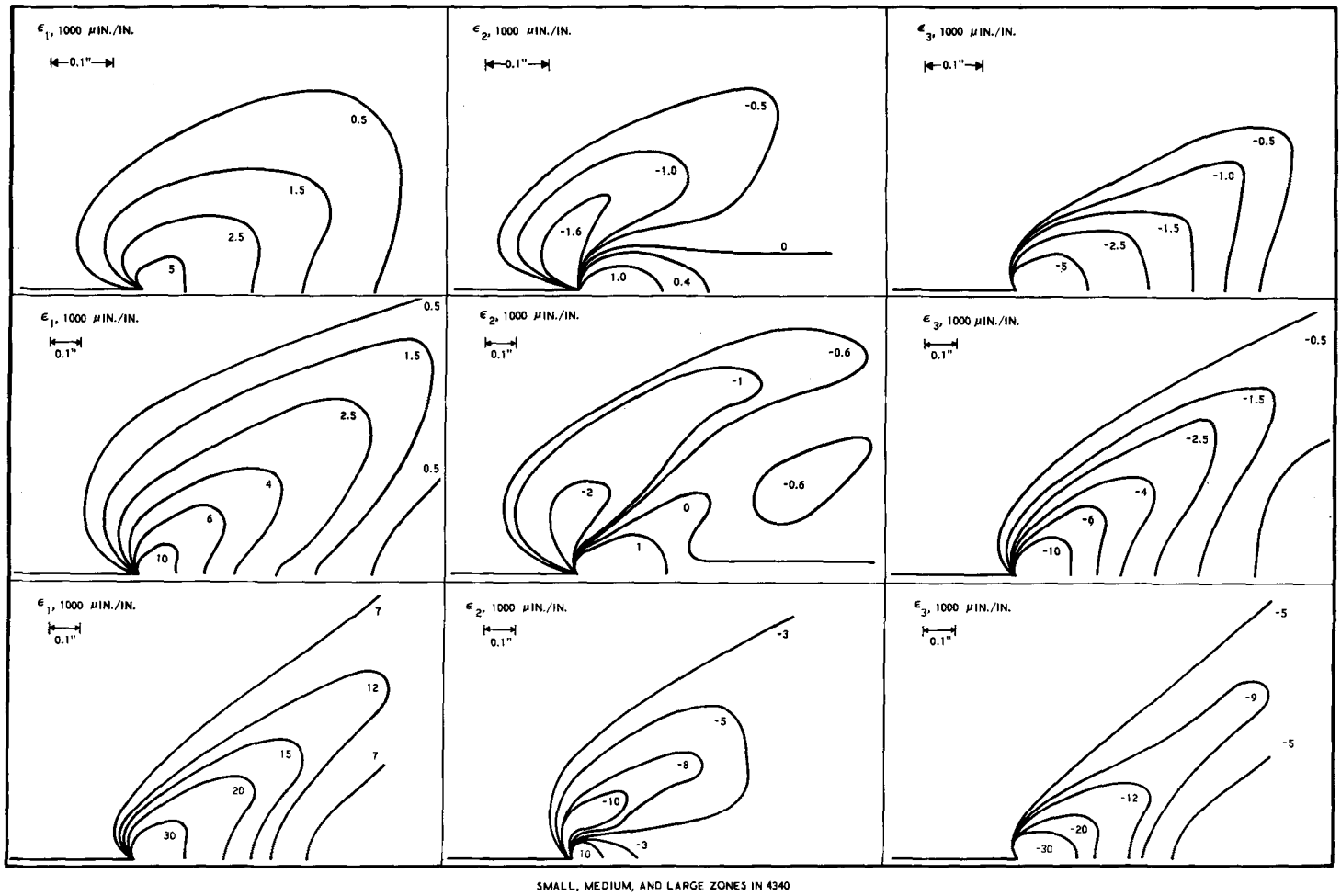

Fig. 8—Principal plastic strain distributions for three enclave sizes of 4340 normalized steel

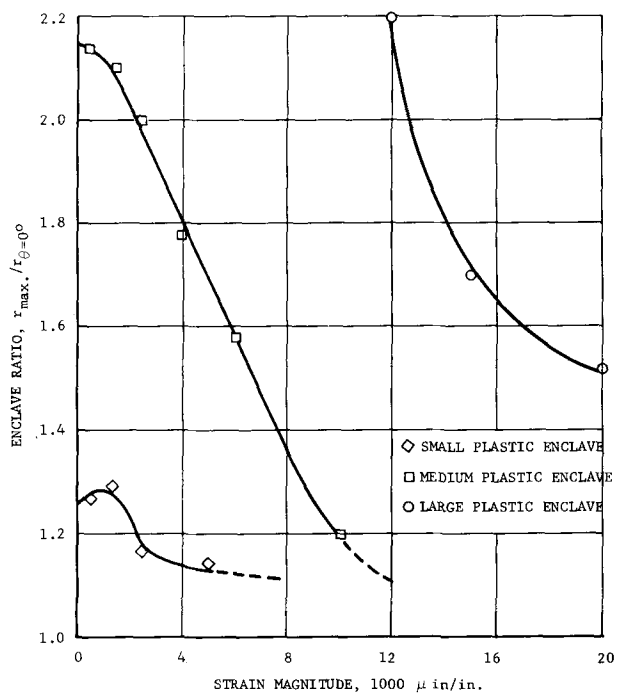

Fig. 9—Variation of enclave shape with enclave size

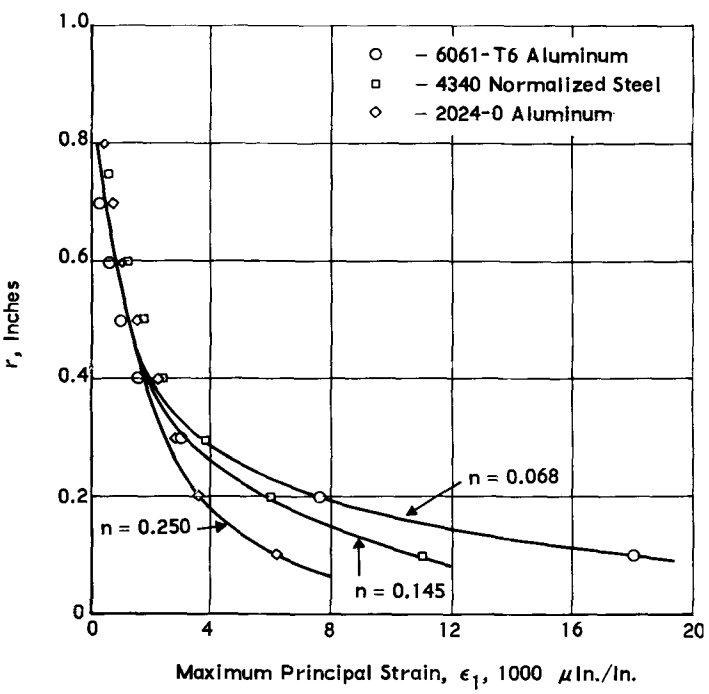

Fig. 10—Effect of strain hardening on maximum principal plastic strain distribution along the line of the crack

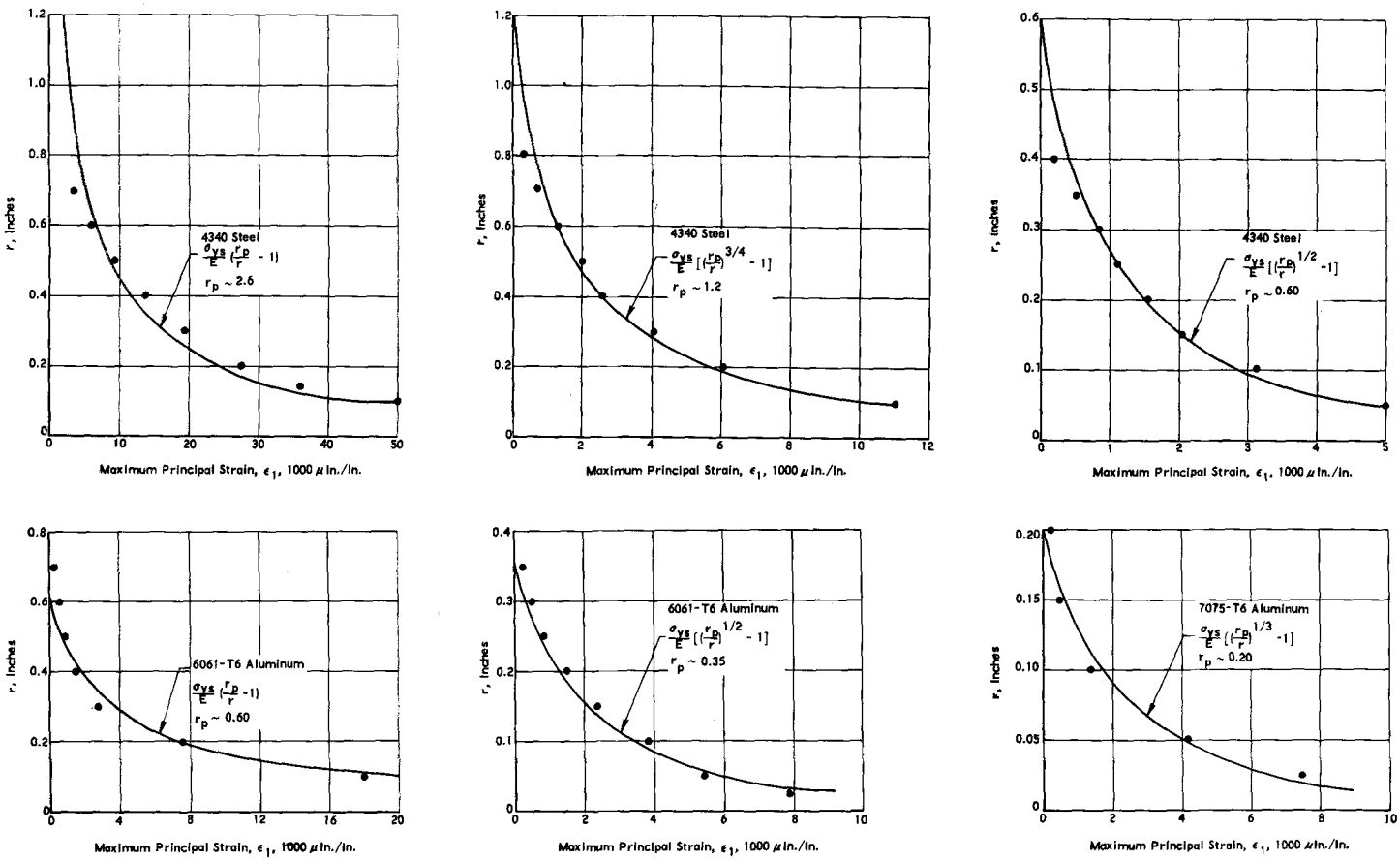

Fig. 11—Effect of enclave size on maximum principal plastic strain distribution along the line of the crack

In Fig. 8, the principal strain distributions for small, medium and large plastic enclaves of 4340 normalized steel are shown. As the enclave size increases, the ϵ_1 and ϵ_3 contours become more pointed. This is similar to the effect of decreasing strain hardening. Also, there is a remarkable similarity between the shape of the small enclave for this medium strain-hardening material and that of the larger enclave for the high strain-hardening 2024-0 aluminum shown in Fig. 5. Thus, the shape of the ϵ_1, ϵ_2 and ϵ_3 distributions for the small enclave of 4340 are also similar to the elastic stress distributions. The large enclave in Fig. 8 is similar in shape to the one obtained for the low strain-hardening material, 6061-T6 aluminum, in Fig. 5. In Fig. 9, a plot of the enclave ratio is made for the three enclave sizes of the 4340 material. For the same strain magnitude, the enclave ratio increases drastically with increasing enclave size. Thus, increasing the size of the enclave and decreasing the strain-hardening properties have similar effects; namely, to cause a greater deviation from the elastic solution. This is intuitive from the shape of the stress–strain curves.

The next point of interest is the effects of strain hardening and enclave size on the strain distribution within the enclave. For three enclaves of about the same size but of different degrees of strain hardening, the extension of the maximum principal strain along the line of the crack is shown in Fig. 10. As the strain hardening increases, the strain magnitude is reduced at a given distance from the crack tip. To obtain a quantitative expression for describing the plastic-strain distribution within the enclaves, Hult and McClintock's[1] analysis for the plastic strain distribution at a crack tip in a non-strain-hardening material under shear is utilized. The tensile analogy gives

$$\epsilon_1 = \frac{\sigma_{ys}}{E}\left(\frac{r_p}{r} - 1\right) \qquad (6)$$

where r_p is an arbitrary value which gives a good fit to the data. It is much closer to the elastic-plastic boundary than the subsequently defined value of r_p' taken at 2000 μin./in. The -1 in eq (6) effectively subtracts the elastic strain. At the left-hand side of Fig. 11, eq (6) fits the data rather well for the relatively large plastic enclaves of two materials. For smaller enclave sizes in each particular material, the strain distribution varies less sharply than r_p/r and tends to approach $(r_p/r)^{1/2}$ which is the type of distribution one might expect from elastic considerations. It should be noted that in Fig. 11 the experimental data are for measurements along the line of the crack. In the case of a small plastic

enclave in 7075-T6 aluminum, the strain distribution varied as $(r_p/r)^{1/3}$ as is seen in the lower right-hand corner of Fig. 11. However, this does not necessarily negate the preceding argument, for it has been shown[18] that the elastic stress distribution determined both experimentally and with numerical solutions[20, 21] varied more closely to $(1/r)^{1/4}$ than to the $(1/r)^{1/2}$ relationship obtained from the one-term elastic solution. Thus, it seems that the plastic strain distribution varies closely to r_p/r for large enclaves and then acquires the characteristics of the elastic-stress distribution with decreasing size.

Having determined the shape of the enclave and how the strain distribution varies within the enclave, it was next necessary to determine how the plastic enclave size varies with material and loading parameters. Referring to Table 2, the enclave size which was measured at the maximum extension of the enclave for ϵ_1 equal to 2000 μin./in. is given for each test coupon. The enclave size was measured at 2000 μin./in. for two reasons. First, there was an uncertainty as to where the elastic-plastic boundary actually was. Second, it was convenient because 2000 μin./in. is the value normally used to define the yield strength of a material with some finite strain hardening. Next, a simple parameter similar to the stress-intensity factor[17] was found to describe the enclave size in terms of the crack length, plate width, applied stress, and yield strength. This dimensionless loading factor is given by

$$F = \left(\frac{\sigma_0}{\sigma_{ys}}\right)^2 \left[\frac{\pi a}{W} + \tan\left(\frac{\pi a}{W}\right)\right] \qquad (7)$$

How the plastic enclave size varies with the loading factor F is shown in Table 2 and in Fig. 12 for the four materials with relative large plastic enclaves. The experimental data show that the enclave size is not a linear function of F but that it increases quite rapidly for values of F much greater than 0.4. It is also seen that the rate of increase of the enclave size is dependent upon the strain-hardening properties of the material. For low strain-hardening materials the enclave size increased quite rapidly, while for high strain-hardening materials, it increased gradually.

With the shape, distribution and size of the plastic enclave fairly well defined, the next thing to consider was the plastic energy within it. First, the plastic-strain energy density, W_d, was determined at each point within the enclave. Three typical results are shown in Fig. 13. Since W_d is roughly proportional to γ_{oct} for low strain hardening materials and since γ_{oct} is fairly linear with ϵ_1 or ϵ_3 when ϵ_2 is small, one would expect the plastic strain energy density contours to be very similar to the ϵ_1 and ϵ_3 principal plastic strain contours. This is indeed observed when comparing Fig. 13 to Fig. 6. A further discussion of strain energy density and its possible use in a ductile failure criterion is given in Part II.[19] With the strain energy density at each mesh point, the total plastic energy for a single enclave (or for half the plate) was determined by the method discussed above. In Table 2, the experimental values of U_p for each specimen are given. It is seen that for a corresponding F value, the low strain-hardening material can absorb considerably more plastic energy. This is more clearly seen in Fig. 14, where the plastic energy is plotted vs. the loading parameter for each material. The effect of strain hardening on the plastic energy absorbed is seen to be similar to its effect on the size of plastic enclave formed. It should be noted that the data in Fig. 14 were normalized for a slight differences of thicknesses using 0.1 in. as the norm.

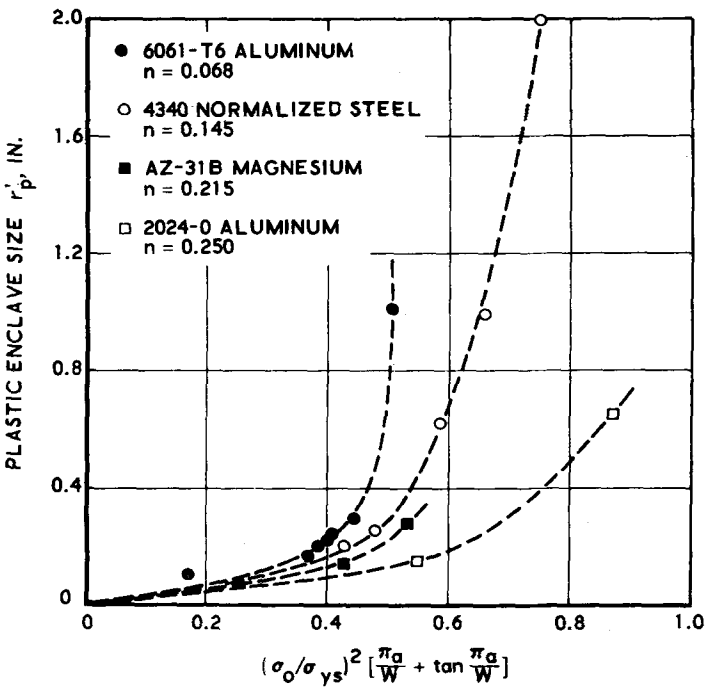

Fig. 12—Effect of loading and strain hardening on plastic enclave size

In this presentation of data, it has been seen how loading and strain hardening affect the principal plastic strain and energy density distributions, and further, how this is reflected in the amount of strain energy that can be plastically absorbed at the crack tip.

Conclusions

1. A technique is presented which allows determination of the principal plastic strains, ϵ_1, ϵ_2 and ϵ_3 within a plastic enclave at a crack tip in thin plates under tensile loading.

2. Consequently, the plastic-strain energy density, W_d, and the total plastic energy, U_p, may be determined in thin plates.

3. It has been clearly shown that the extent of plastic deformation and strain hardening have a major influence on the size, shape and orientation of plastic enclaves and the strain distribution within them.

4. The smaller the strain hardening and/or the

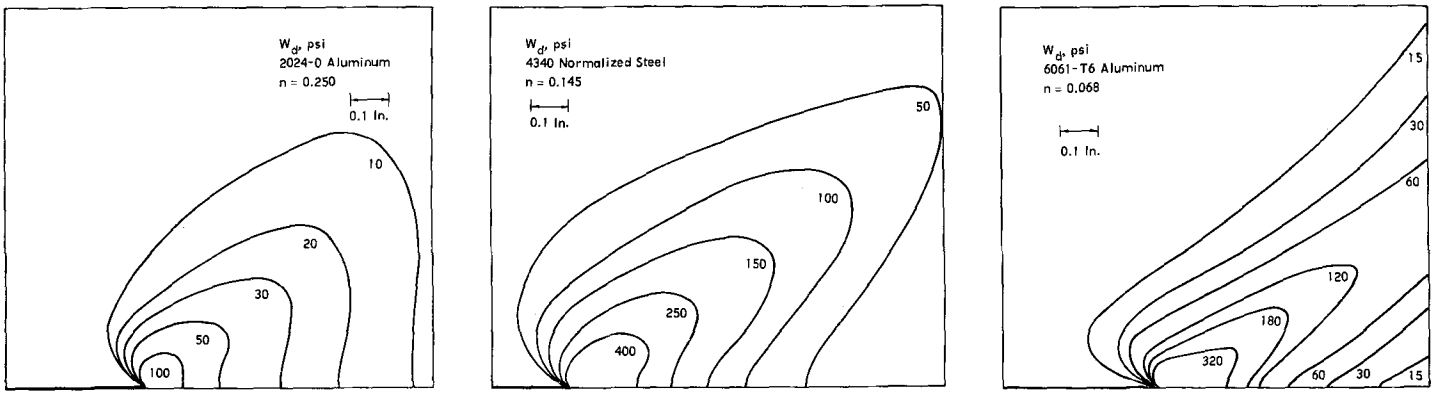

Fig. 13—Plastic distortional strain energy density distributions for 2024-0 aluminum, 4340 normalized steel and 6061-T6 aluminum

larger the enclave size, the more pinched and distended the plastic enclaves become.

5. Within the enclave, the maximum principal strain distribution varies as r_p/r for relatively large enclaves and $(r_p/r)^{1/2}$ for relatively small ones.

6. The shape of the plastic strain energy density contours are very similar to the maximum principal strain contours, ϵ_1 and ϵ_3.

7. For an equivalent loading condition, a low strain-hardening material will have a larger plastic enclave and hence absorb much more energy plastically than a high strain-hardening material.

Acknowledgment

The experimental investigation was initiated at the Jet Propulsion Laboratory under NASA Contract NAS 7-100; the majority of the program was supported by and completed at Philco Research Laboratories Division of Philco Corp., a subsidiary of Ford Motor Co. The photograph in Fig. 4, shown through the courtesy of J. R. Dixon,[8] is released by "Crown Copyright. Reproduced by permission of the Controller of H. M. Stationery Office, East Kilbride, Glasgow."

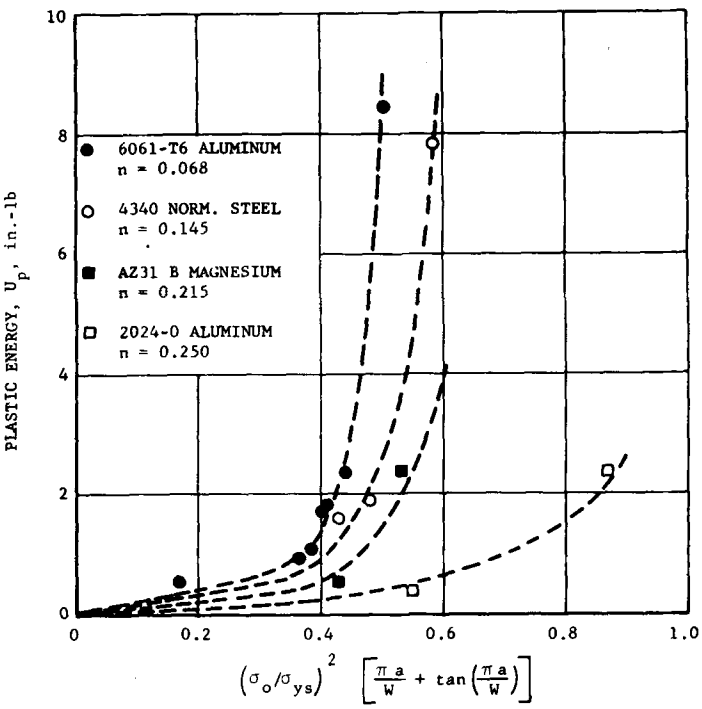

Fig. 14—Effect of loading and strain hardening on plastic energy absorption

References

1. *Hult, J. and McClintock, F., "Elastic-Plastic Stress and Strain Distributions Around Sharp Notches Under Repeated Shear," Ninth Internat. Cong. Appl. Mech., Brussels, 8, 51–58 (1956).*
2. *McClintock, F., "Ductile Fracture Instability in Shear," Jnl. Appl. Mech., Trans. ASME, 80, 582–588 (December 1958).*
3. *Koskinen, M., "Elastic-Plastic Deformation of a Single Grooved Flat Plate Under Longitudinal Shear," ASME Paper 62-WA-137, to be published in the Jnl. Basic Eng.*
4. *Allen, D. de G. and Southwell, R., "Plastic Straining in Two-Dimensional Stress Systems," Philos. Trans. Royal Soc., London, Series A, 242, 379–414 (1950).*
5. *Stimpson, L. and Eaton, D., "The Extent of Elasto-Plastic Yielding at the Crack Point of an Externally Notched Plane Stress Tensile Specimen," ARL 24, Aeron. Res. Lab., OAR 1961.*
6. *Jacobs, J., "Relaxation Methods Applied to Problems of Plastic Flow I. Notched Bar Under Tension," Philos. Mag., 41, 349–361 (1950).*
7. *Kawata, K., "Analysis of Elasto-Plastic Behavior of Metals by Means of Photoelastic Coating Method," Jnl. Sci. Res. Inst., Tokyo, 52, 17–40 (1958).*
8. *Dixon, J., and Visser, W., "An Investigation of the Elastic-Plastic Strain Distribution Around Cracks in Various Sheet Materials," Proc. Internat. Symp. Photoelasticity, Chicago, 1961, Pergamon Press 1963.*
9. *Ault, R. and Spretnak, J., "Initial Yielding and Fracture in Notched Sheet Molybdenum," Report ASD-TDR 62-223, Wright Field, April 1962.*
10. *Liu, S. and Carpenter, S., "A Study of Plastic Deformation and Fracturing by Strain Energy Distribution; Internally Notched Steel Plates Under Tension," Progress Report, Ship Structure Committee Serial No. SSC-38, Swarthmore College, December 1950.*
11. *Weiss, V., Grewal, K., Sachs, G., Sessler, J., "A Study of Plastic Deformation in Flat Notch Tension Specimens as Function of Strength Level and Initial Stress Concentration Factor," Report Met. E-604-6012F II, Syracuse Univ. Res. Inst., December 1960.*
12. *Inglis, C., "Stresses in a Plate Due to the Presence of Cracks and Sharp Corners," Trans. Inst. Naval Arch., London, 60, 219 (1913).*
13. *Westergaard, H., "Bearing Pressures and Cracks," Jnl. Appl. Mech. Trans. ASME, 61, A-49–A-53 (1939).*
14. *Williams, M., "On the Stress Distribution of the Base of a Stationary Crack," Jnl. Appl. Mech., Trans. ASME, 79, 109–114 (March 1957).*
15. *Griffith, A., "The Phenomenon of Rupture and Flow in Solids," Philos. Trans. Royal Soc., London, Series A, 221, 163 (1921).*
16. *Orowan, E., "Fundamental of Brittle Behavior in Metals," Fatigue and Fracture Metals, Technology Press, M.I.T., 1952.*
17. *Irwin, G., "Analyses of Stresses and Strains Near the End of a Crack Traversing a Plate," Jnl. Appl. Mech., Trans. ASME, 79, 361–364 (1957).*
18. *Gerberich, W., "Stress Distribution About a Slowly Growing Crack Determined by Photoelastic-Coating Method," Proc. SESA, XIX (2), 359–365 (1962).*
19. *Swedlow, J. and Gerberich, W., "Plastic Strains and Energy Density in Cracked Plates: II Comparison to Elastic Theory," to be published in December 1964 issue of* EXPERIMENTAL MECHANICS.
20. *Stimpson, L., Personal Communication, Calif. Inst. Tech. 1961.*
21. *Redshaw, S., and Rushton, K., "An Electrical Analogue Solution for the Stresses Near a Crack or a Hole in a Flat Plate," Jnl. Mech. Phys. Solids, 8, 178–187 (1961).*